

# Multiple intermediates in SNARE-induced membrane fusion

Tae-Young Yoon\*, Burak Okumus†, Fan Zhang‡, Yeon-Kyun Shin\*§, and Taekjip Ha\*†§¶

\*Howard Hughes Medical Institute, †Center for Biophysics and Computational Biology, and ¶Department of Physics, University of Illinois at Urbana–Champaign, Urbana, IL 61801; and ‡Department of Biochemistry, Biophysics, and Molecular Biology, Iowa State University, Ames, IA 50011

Edited by Thomas C. Südhof, University of Texas Southwestern Medical Center, Dallas, TX, and approved October 31, 2006 (received for review July 18, 2006)

Membrane fusion in eukaryotic cells is thought to be mediated by a highly conserved family of proteins called SNAREs (soluble *N*-ethyl maleimide sensitive-factor attachment protein receptors). The vesicle-associated v-SNARE engages with its partner t-SNAREs on the target membrane to form a coiled coil that bridges two membranes and facilitates fusion. As demonstrated by recent findings on the hemifusion state, identifying intermediates of membrane fusion can help unveil the underlying fusion mechanism. Observation of SNARE-driven fusion at the single-liposome level has the potential to dissect and characterize fusion intermediates most directly. Here, we report on the real-time observation of lipid-mixing dynamics in a single fusion event between a pair of SNARE-reconstituted liposomes. The assay reveals multiple intermediate states characterized by discrete values of FRET between membrane-bound fluorophores. Hemifusion, flickering of fusion pores, and kinetic transitions between intermediates, which would be very difficult to detect in ensemble assays, are now identified. The ability to monitor the time course of fusion events between two proteoliposomes should be useful for addressing many important issues in SNARE-mediated membrane fusion.

FRET | single-molecule spectroscopy | lipid mixing

Single-liposome fluorescence imaging (1–5) is a powerful method for observing and dissecting the fusion dynamics of biological membranes (6–8). Because it can follow directly the time course of a single reaction without the need for synchronization, the single-liposome approach has the potential to clarify important issues that spatiotemporal averaging in ensemble measurements cannot.

Soluble *N*-ethyl maleimide sensitive-factor attachment protein receptor (SNARE) proteins are involved in membrane fusion during exocytosis and vesicular trafficking (9–11). Recent studies provided evidence that SNARE-mediated fusion transits through hemifusion (12–15) (however, see also ref. 16), similar to the fusion pathway proposed for type I (17, 18) and II viruses (19, 20) and lipidic membrane fusion (1, 21). Hemifusion is a metastable membrane structure in which the outer leaflets are merged but the inner leaflets remain intact (22). It has been shown that the rate of inner leaflet mixing is slower than that of outer leaflet mixing in a SNARE-reconstituted fusion reaction (15). The lipid mixing was also shown to occur earlier than aqueous content mixing in fusion between native vacuoles (14). These results are in favor of the mechanism through hemifusion (22). However, an alternative mechanistic model in which hemifusion is designated as an off-pathway state that can be reversed by liposomes detachment can explain the results equally well (15). This issue of hemifusion along with many other compelling questions surrounding the topic of SNARE-induced membrane fusion may be clearly addressed by observing a fusion event at the level of single liposomes.

We have established a fluorescence-based single liposome fusion assay that enables us to monitor lipid mixing between two proteoliposomes in real time. Previous approaches have been focused on fusion of single liposomes with larger-scale membranes such as

supported (1–4) or plasma membranes (5). The fluorophores contained in single liposomes then inevitably diffuse away subsequent to fusion. In contrast, the fusing objects in our assay, two proteoliposomes, constitute a small closed system. The number of fluorophores therefore is preserved throughout the fusion process such that each fusion intermediate with a certain degree of lipid mixing corresponds to a discrete FRET value. The dwell time in each intermediate can also be precisely determined. As a result, the complete lipid-mixing dynamics of SNARE-mediated fusion, that is, from docking to full fusion, has been monitored and dissected in detail.

## Results and Discussion

### Single-Liposome FRET Assay for SNARE-Induced Membrane Fusion.

Liposome fusion mediated by recombinant SNAREs, Sso1pHT, Sec9c, and Snc2pF, which are involved in trafficking from Golgi to the plasma membrane in yeast was imaged by using total internal reflection FRET microscopy (Fig. 1*a*) (23–25). Sso1pHT (the yeast counterpart of neuronal t-SNARE syntaxin) was reconstituted into unilamellar liposomes {1-palmitoyl-2-oleoyl-*sn*-glycero-3-phosphocholine (POPC)/1,2-dioleoyl-*sn*-glycero-3-[phospho-L-serine] (DOPS) (mol/mol) = 65:35} that contain the membrane-intercalating fluorescent donor 1,1'-dioctadecyl-3,3,3',3'-tetramethylindocarbocyanine perchlorate (DiI) (2 mol%). Another t-SNARE Sec9c (neuronal SNAP-25 analogue) was prepared as a soluble protein and added to the Sso1pHT-proteoliposomes to form t-SNARE liposomes. The v-SNARE Snc2pF (neuronal synaptobrevin analogue) was reconstituted into a separate population of unilamellar liposomes that contain the membrane fluorescence acceptor 1,1'-dioctadecyl-3,3,3',3'-tetramethylindocarbocyanine perchlorate (DiD) (2 mol%) and biotinylated lipids (0.1 mol%). Lipid-to-protein ratio was kept at 100:1, and proteoliposome diameter was 94 ( $\pm$ 23) nm as determined by electron microscopy (Fig. 1*b*).

The v-SNARE liposomes were attached to a quartz surface coated with PEG (23), which eliminates nonspecific surface adhesion of liposomes. Immobilization was achieved by biotinylated

Author contributions: T.-Y.Y., B.O., and F.Z. contributed equally to this work; Y.-K.S. and T.H. designed research; T.-Y.Y., B.O., and F.Z. performed research; Y.-K.S. and T.H. contributed new reagents/analytic tools; T.-Y.Y. analyzed data; and T.-Y.Y., Y.-K.S., and T.H. wrote the paper.

The authors declare no conflict of interest.

This article is a PNAS direct submission.

Freely available online through the PNAS open access option.

Abbreviations: SNARE, soluble *N*-ethyl maleimide sensitive-factor attachment protein receptor; DiI, 1,1'-dioctadecyl-3,3,3',3'-tetramethylindocarbocyanine perchlorate; DiD, 1,1'-dioctadecyl-3,3,3',3'-tetramethylindocarbocyanine perchlorate; PE, phosphatidylethanolamine.

See Commentary on page 19611.

§To whom correspondence may be addressed. E-mail: colishin@iastate.edu or tjha@uiuc.edu.

This article contains supporting information online at [www.pnas.org/cgi/content/full/0606032103/DC1](http://www.pnas.org/cgi/content/full/0606032103/DC1).

© 2006 by The National Academy of Sciences of the USA

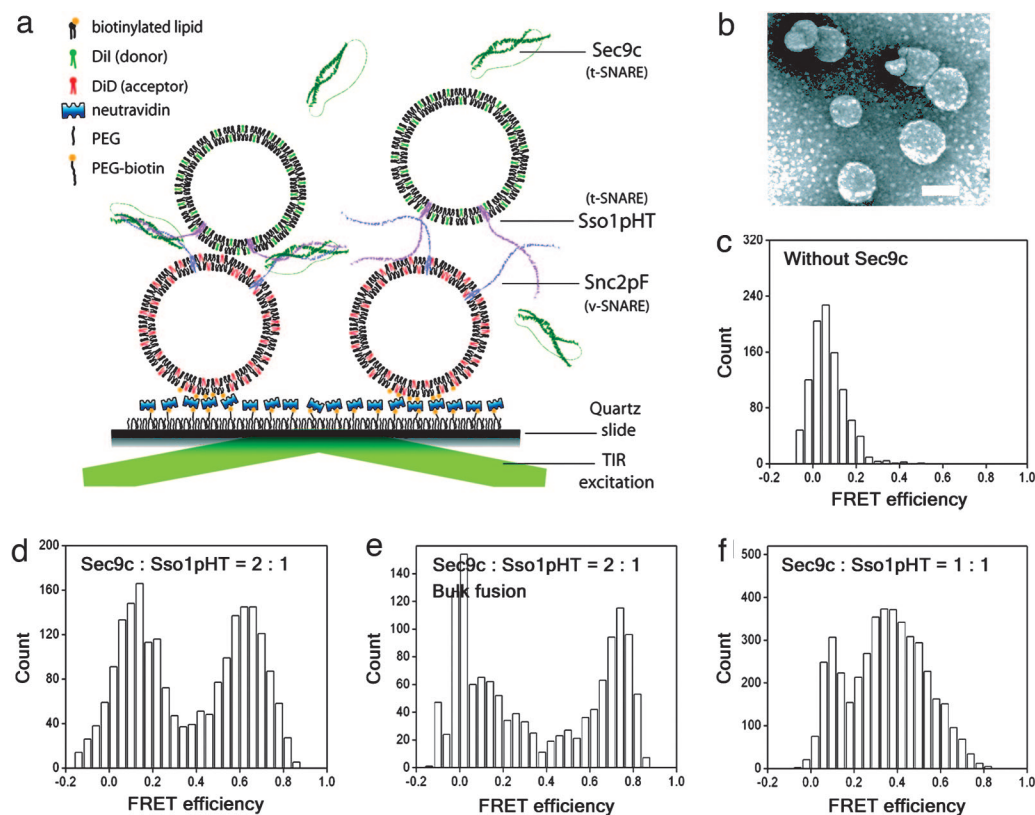


**Fig. 1.** Single-liposome fluorescence assay of SNARE-mediated membrane fusion. (a) Schematics of the assay. The v-SNARE liposomes containing membrane fluorescent acceptors are tethered on a PEG-coated quartz slide, and Sso1pHT-reconstituted liposomes doped with membrane fluorescent donors are introduced together with Sec9c to induce fusion. The mixing of donor and acceptor dyes caused by fusion between the cognate liposomes leads to increase in  $E$ , which is being monitored by wide-field total internal reflection (TIR) microscopy. (b) Negative staining electron micrograph of the Sso1pHT-reconstituted liposomes (1200 EX; JEOL, Tokyo, Japan). (Scale bar: 100 nm.) (c–f) Final  $E$  distribution of the products of SNARE-driven single-liposome fusion (after 30 min of reaction) in the absence of Sec9c (c) and at the Sec9c/Sso1pHT ratio of 2:1 (d and e) and 1:1 (f). The fusion reactions of c, d, and f were induced on surface (as illustrated in a), whereas in e, fusion was induced in bulk solution and the products were subsequently immobilized on the quartz surface for observation. We notice that after 30 min of reaction the fraction of the population that remains at the docked state varies significantly sample by sample.

lipids on the liposome and PEG-bound neutravidins (Fig. 1a). Then, the t-SNARE liposomes were flowed in at 100  $\mu$ M concentration at 37 ( $\pm$ 2)  $^{\circ}$ C, while donor and acceptor fluorescence from single liposomes was being recorded with 100- or 900-ms time resolution. The very low concentration of t-SNARE liposomes minimizes interaction of multiple t-SNARE liposomes with a single v-SNARE liposome. Because the direct excitation of the acceptor fluorophores in the v-SNARE liposomes (with 532-nm laser wavelength used) was negligible, we did not see appreciable fluorescence signal until a t-SNARE liposome docked to a v-SNARE liposome. Lipid mixing between the two liposomes caused by fusion would lead to an increase in FRET efficiency,  $E$ , defined as  $I_A/(I_D + I_A)$ , where  $I_D$  and  $I_A$  are the donor and the acceptor fluorescence intensities, respectively (23–25). We assume that there is only a single productive fusion site per pair of liposomes, which is reasonable considering the small size of the liposomes.

**Calibration of FRET Efficiency.** Sec9 is known to be required for yeast SNARE-mediated membrane fusion (26). The conventional ensemble fusion assay of our t- and v-SNARE liposomes also clearly shows that Sec9c is essential for inducing membrane fusion in solution [supporting information (SI) Fig. 5]. We tested whether the same is true here for our single-liposome fusion assay. In the absence of Sec9c, we observed a final  $E$  distribution centered at  $\approx$ 0.08 and all  $<$ 0.25 (Fig. 1c; obtained after 30 min of reaction). The finite but low  $E$  values suggest close contact or docking between the donor and the acceptor liposomes without a high degree of lipid

mixing between the liposomes (state D in Fig. 2k and see SI Fig. 6 for individual fluorescence time traces). In contrast, inclusion of Sec9c in the reaction [Sec9c/Sso1pHT (mol/mol) = 2:1] led to a major population at  $E = 0.67$  in the final  $E$  distribution (Fig. 1d; obtained after 30 min of reaction), indicating significant lipid mixing. The relatively broad  $E$  distribution can be attributed to size variation of liposomes and measurement noise. When the v- and t-SNARE liposomes were allowed to fuse in bulk solution (see *Materials and Methods*) and later adhered on the surface, the  $E$  distribution was very similar to that of fusion induced on the surface except for a small shift in the peak to  $E \approx 0.75$  (Fig. 1e). In addition, protein-free liposomes with 1% mol of DiI and DiD, which would approximate the completely mixed liposomes, gave a peak at a similar  $E$  value ( $\approx$ 0.8) (SI Fig. 7). Therefore, our single liposome assay faithfully recapitulates the main features of SNARE-mediated fusion in solution, including the requirement of Sec9c, and we assign the  $E \approx 0.65$  as an indicative of full fusion where both inner and outer leaflets have been mixed (state F in Fig. 2k). The slight lower  $E$  values for fusion reactions on the surface may possibly be caused by the acceptor fluorophores that are confined at the immobilization site crowded with neutravidin molecules (27).

If a lower Sec9c concentration was used (Sec9c/Sso1pHT = 1:1), the final  $E$  distribution showed a major peak at  $E = 0.35$  instead (Fig. 1f), indicating that SNARE-induced fusion can produce final states different from full fusion. Because bulk solution studies detected primarily hemifusion when low protein concentration was used (12, 18), we tentatively assign  $E = 0.35$  to hemifusion and set

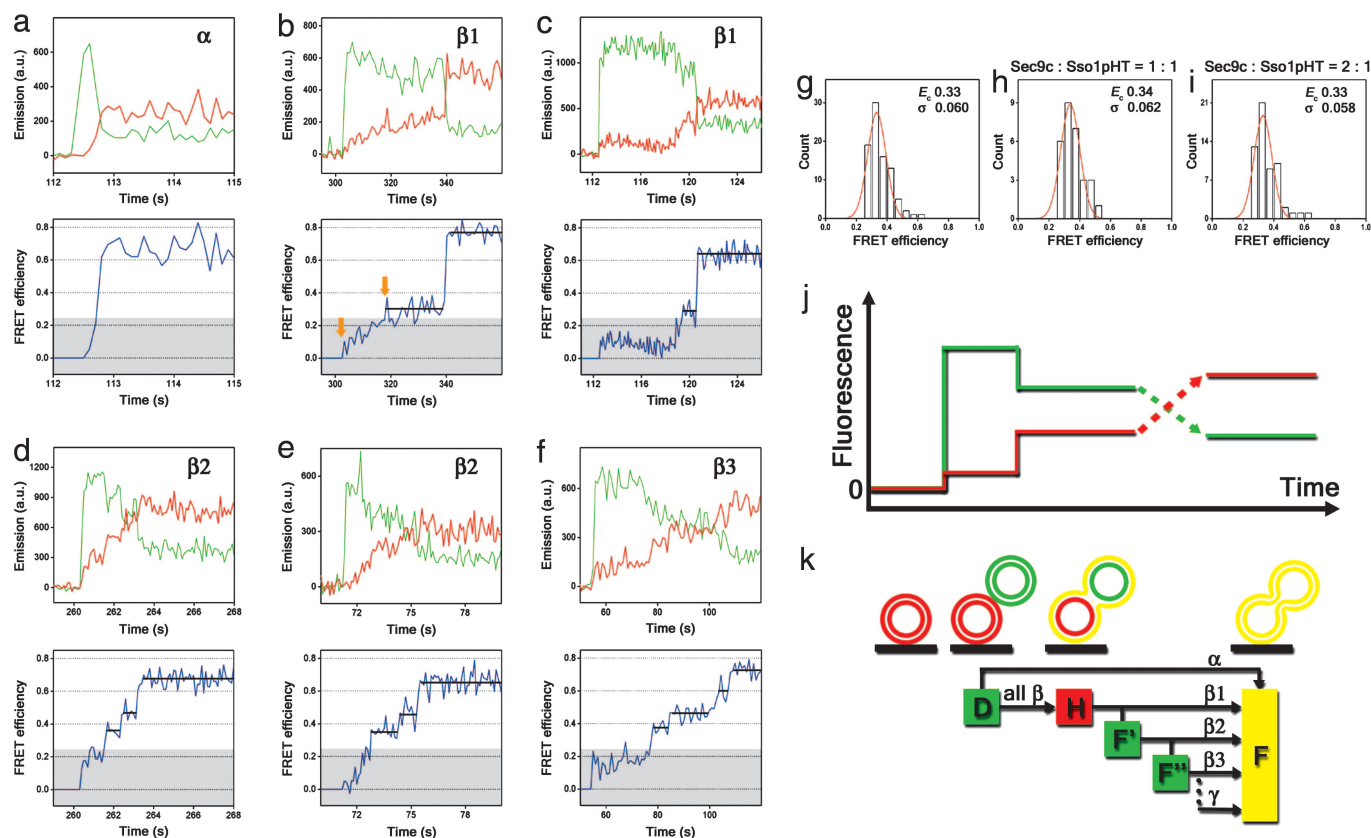


**Fig. 2.** Multiple intermediate states of SNARE-induced fusion. (a–f) Single-liposome fusion time traces; full fusion events with no intermediates (classified as  $\alpha$  class, a), one intermediate state ( $\beta_1$  class, b and c), two intermediate states ( $\beta_2$  class, d and e), and three intermediate states ( $\beta_3$  class, f). (Upper) Shown is the fluorescence intensity time traces of the donor ( $I_D$ , green) and the acceptor ( $I_A$ , red) channels. (Lower) Shown is the corresponding FRET efficiency (blue) where the intermediate states are marked with black bars. In b, docking of a t-SNARE liposome is followed by a gradual FRET increase (between the two arrows), which culminates with the first intermediate state. (g–i) FRET histograms of the first intermediate state for the subclasses  $\beta_1$ ,  $\beta_2$ , and  $\beta_3$  (g). The narrow distribution is not disturbed when traces obtained at the different Sec9c/Sso1pHT ratios of 2:1 (h) and 1:1 (i) are separately considered. The histograms are fitted with the Gaussian distributions, and the center ( $E_c$ ) and the standard deviation ( $\sigma$ ) of the Gaussians are shown. (j) Schematic illustration of a typical single-liposome fusion time trace. (k) Pathway of SNARE-driven membrane fusion. For the class  $\beta$ , docking of a t-SNARE liposome and close contacting between two liposomes (state D) are followed by an obligatory intermediate state, the hemifusion state (state H). The number of premature closings of the fusion pore ( $F'$ ,  $F''$ , and so on) between the hemifusion state and the full fusion state (state F) then determines the subclass such as  $\beta_1$ ,  $\beta_2$ , and  $\beta_3$ . Class  $\alpha$  evolves from the D to F state without discernible intermediate states. In contrast, the FRET increase of class  $\gamma$  is too gradual for intermediates to be identified, which could be caused by many pore-flickering phenomena.

a threshold at  $E = 0.5$  for deciding whether full fusion has occurred or not. Our assignment is also supported by observing fusion between phosphatidylethanolamine (PE)-containing vesicles. A PE lipid molecule has a small head group compared with its hydrocarbon chains, thus creating a spontaneous curvature that helps the formation of the hemifusion state but suppresses the following steps including opening of fusion pores (28). With 30 mol% PE composition, resultant final  $E$  distribution after 30 min of reaction showed significantly enhanced population between 0.25 and 0.44 at the expense of populations with  $E > 0.5$ , which is greatly diminished (SI Fig. 8), suggesting again that the hemifusion state has  $E \approx 0.35$ .

**Observing Single-Liposome Fusion Dynamics in Real Time.** Single-liposome fusion time traces shown in Fig. 2 a–f demonstrate key advantages of our assay; docking can be clearly distinguished from subsequent fusion and reaction intermediates can be seen directly. Docking of a t-SNARE liposome to a surface-tethered v-SNARE liposome is observed as an abrupt increase of the donor fluorescence intensity,  $I_D$ , and the FRET efficiency monotonically increases with increasing lipid mixing (observed as an increase in  $I_A$  accompanied by a concomitant decrease in  $I_D$ ) (Fig. 2j and SI Movie 1). Additional docking by another t-SNARE liposome can be ruled out as such an event would display a further sharp increase

in  $I_D$ , which was not observed at the low liposome concentration used (100 pM). The average time between addition of t-SNARE liposomes to the sample and individual docking was 240 s (SI Fig. 9), far slower than the subsequent fusion steps (see Fig. 3). It is likely that the ensemble fusion kinetic curve (SI Fig. 5) primarily reflects the kinetics of docking. Therefore, detailed fusion reaction intermediates would have been very difficult to detect without the postsynchronization (29) afforded by our single-liposome fusion assay.

Of total 314 fusion time traces obtained with both 2:1 and 1:1 ratios of Sec9c/Sso1pHT, 160 traces were classified as the full fusion traces (final  $E > 0.5$ ). Three broad classes of the full fusion traces were identified: ( $\alpha$ ) direct full fusion without discernible intermediate FRET states above  $E = 0.25$  (33%,  $n = 53$ ; Fig. 2a), ( $\beta$ ) full fusion with one or more discrete intermediate plateaus (or steps) with  $E > 0.25$  (54%,  $n = 87$ ; Fig. 2 b–f and see SI Fig. 10 for more traces), and ( $\gamma$ ) full fusion with intermediate FRET values above  $E = 0.25$  but without discernible plateaus (13%,  $n = 20$ ; see SI Fig. 11 for fusion time traces). We did not assign FRET values  $< 0.25$  (marked with the gray boxes in Fig. 2 a–f) to fusion intermediates because these values were observed even in the absence of Sec9c and therefore could not be unambiguously distinguished from close docking of liposomes. The majority class  $\beta$  can be further divided

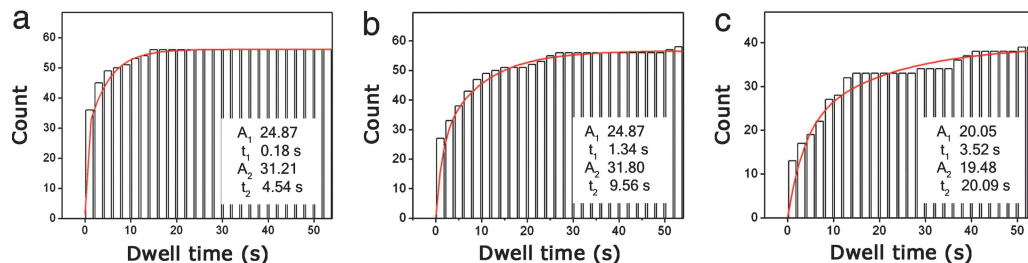


**Fig. 3.** Kinetic analysis of single-liposome fusion time traces. In this analysis, only the class  $\beta$  ( $\beta_2$  and  $\beta_3$  in the case of the second intermediate) obtained at the Sec9c/Sso1pHT ratio of 2:1 was used. Shown are cumulative dwell time histograms of docked (a), first intermediate (b), and second intermediate (c) states. The docked state is defined as an intermediate plateau with the largest  $E < 0.25$ . With the first-order kinetics assumed, the dwell time histograms are fitted by using two exponentials,  $A_1(1 - \exp^{-t/t_1}) + A_2(1 - \exp^{-t/t_2})$  (red curve). (Insets) The dwell times ( $t_1$ ,  $t_2$ ) and the corresponding number of traces ( $A_1$ ,  $A_2$ ) are shown.

according to the number of discrete intermediate steps above  $E = 0.25$ : ( $\beta_1$ ) one intermediate step ( $n = 28$ ; Fig. 2 b and c), ( $\beta_2$ ) two intermediate steps ( $n = 47$ ; Fig. 2 d and e), and ( $\beta_3$ ) three intermediate steps ( $n = 12$ ; Fig. 2f). Thus, our single-liposome assay can identify multiple intermediate steps toward full fusion, providing an opportunity to dissect the pathways and kinetics of SNARE-induced fusion.

The FRET histogram of the first intermediate step for all subclasses  $\beta_1$ ,  $\beta_2$ , and  $\beta_3$  is narrowly peaked at  $E = 0.33$  (standard deviation,  $\sigma = 0.06$ ) (Fig. 2g), regardless of the Sec9c/Sso1pHT ratio (Fig. 2 h and i). Thus,  $E = 0.33$  state can be considered an obligatory intermediate for the majority of full fusion events (that is, in the class  $\beta$ ). Furthermore, we observed a major population at  $E = 0.35$  at a low Sec9c concentration (Fig. 1f) or with PE-containing vesicles (SI Fig. 8), which was known to favor hemifusion as the final product. Based on these observations, it is highly likely that the first intermediate step at  $E = 0.33$  represents the hemifusion intermediate (state H in Fig. 2k). Our result is direct evidence that the hemifusion state is the *de facto* on-pathway intermediate in SNARE-induced fusion instead of being a dead-end product.

Next, we discuss the observation of additional intermediates beyond hemifusion, an unexpected finding that would have been hidden in ensemble fusion experiments. Previous studies suggest that hemifusion could be followed by fusion pore formation and that the pore may close prematurely before inner leaflet lipid mixing is completed (30, 31). Our data are consistent with such a model of fusion pore flickering provided that the pore closing occurs on a similar time scale to that of complete lipid mixing through an open pore, which would be on the order of 1 ms for unrestricted diffusion of lipids over the liposome surface. Then, the subclass  $\beta_1$  would reflect a single fusion pore formation event leading to complete fusion within our time resolution. Likewise,  $\beta_2$  would be caused by a premature closing of the pore after partial lipid mixing (state F' in Fig. 2k), which then requires an additional pore opening for complete mixing, and  $\beta_3$  with two premature closings (state F' and F'' in Fig. 2k) and so on. It is plausible that fusion events with more pore flickering ( $\beta_4$ ,  $\beta_5$ , ...) could not be detected because of the limited signal-to-noise ratio and time resolution, and such cases may be responsible for the class  $\gamma$  fusion trajectories, which do not show discernible steps (Fig. 2k). These effects we attributed to fusion pore flickering could in principle be caused by a new assembly of fusion complexes instead of being mediated by those formed during hemifusion. This possibility, however, is less likely because of a small area of contact between the two small liposomes.

**Dwell Time Analysis of Single-Liposome Fusion.** To gain further insight into the underlying mechanism of these additional intermediates, we carried out the dwell time analysis of the docked state, and the first (state H) and the second (state F') intermediate steps. Cumulative dwell time plots show that both the first and the second intermediate steps have longer dwell times ( $t_1$ ,  $t_2$ ) than the docked

state (Fig. 3). According to the fusion pore flickering model discussed above, both dwell times in the first and the second intermediate steps would be the latent times for opening a fusion pore. Then, it would imply that fusion pore formation after hemifusion faces a larger energetic barrier than hemifusion itself (32, 33). In fact, typically  $<20\%$  of the total time required for full fusion is spent between docking and hemifusion (SI Fig. 12), probably suggesting that fusion pore opening is the most time-consuming step.

Fig. 3 also shows that the dwell time distributions are not simple exponentials. At least double exponential decay functions were needed to fit the data adequately, indicating a heterogeneous population. Because of the limited observation time (100 ms to hundreds of s), extremely fast or slow lipid mixing dynamics could not be monitored, and the heterogeneity in reaction kinetics may even be more extensive than implied by the double exponential fits. We do not yet understand the origin of the heterogeneity, but one possibility is the variation in the number of active SNARE proteins per liposome. Class  $\alpha$ , which shows full fusion without the hemifusion intermediate, may indeed contain more active SNARE proteins than average so that the fusion pore opening from the hemifusion state is extremely rapid. However, we cannot technically rule out the possibility that up to one-third of the full fusion events may proceed through a separate pathway that does not involve hemifusion. Observing the single fusion events with a better temporal resolution may be able to reveal whether all SNARE-induced fusion events proceed through hemifusion.

**Partially Restricted Hemifusion and Kiss-And-Run-Like Events.** Time traces of single-liposome fusion also reveal additional features. For example, in a small number of traces, a gradual FRET increase precedes the hemifusion plateau (between the arrows in Fig. 2b; see SI Fig. 13 for more fusion traces). That is, hemifusion may not be achieved in a single step for some cases. We suggest three possibilities. The first is the existence of "partially restricted" hemifusion state (18) in SNARE-mediated fusion, where lipid mixing is suppressed by a ring-like arrangement of SNARE complexes, which lines the junction of the t- and v-SNARE liposomes. The second is fast flickering during the formation of the hemifusion state as suggested in a previous ensemble study (15). Such an effect may be responsible for some docked states with the FRET value as large as  $\approx 0.2$ . The third possibility is a disorganized lipid mixing process caused by a random arrangement of SNARE complexes.

We have also observed kiss-and-run-like events (30, 31) in which total fluorescence signal abruptly decreases after full or nearly full fusion, presumably caused by the detachment of what remains of the t-SNARE liposome from the v-SNARE liposome ( $n = 4$ ; Fig. 4). No such decrease in total fluorescence was observed in the hemifusion or docked states. There is no accompanying FRET change upon such kiss-and-run type of detachment, suggesting that both liposomes have the same degree of lipid mixing upon completion of fusion.

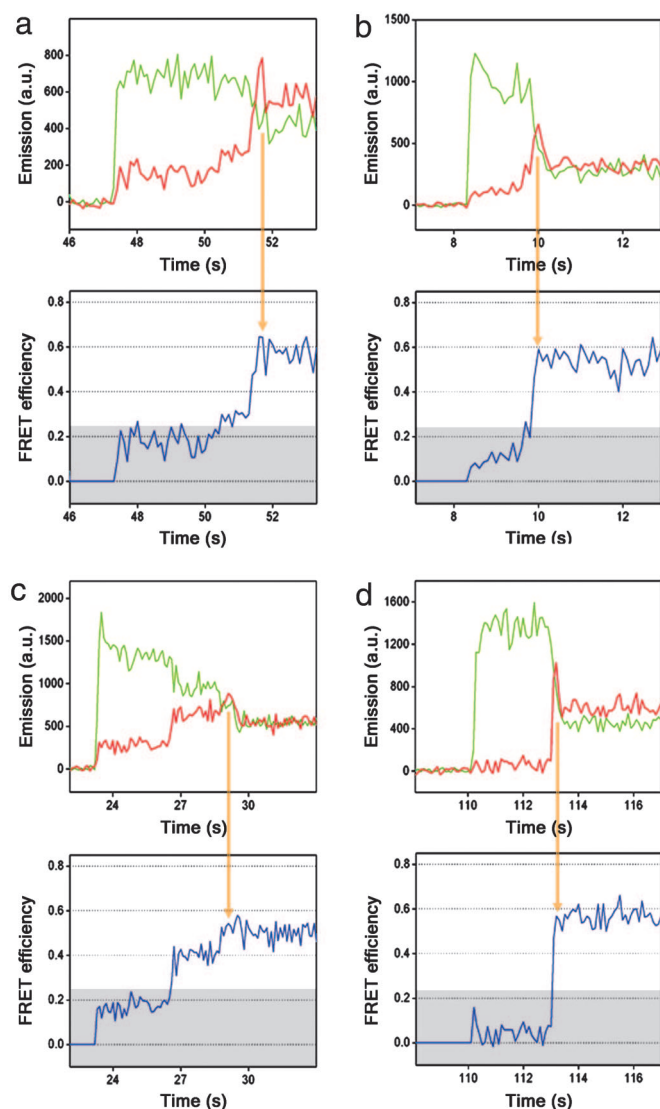


**Fig. 4.** Kiss-and-run-like fusion events. Shortly after the fusion-pore opening, which leads to complete lipid mixing, both the donor and acceptor fluorescence signals decrease without appreciable changes in the FRET efficiency for the class  $\beta$  (a and c) and the class  $\alpha$  (b and d). Such an effect is consonant with the detachment of what remains of the t-SNARE liposome. (Upper) Shown are the changes in the donor (green) and the acceptor (red) fluorescence intensities. (Lower) The corresponding changes in the FRET efficiency (blue) are shown.

## Conclusions

Our approach described here provides a general avenue for observing single-liposome fusion events in proteoliposome systems (9, 12, 15, 34–36). Modification of the more conventional bulk-phase assays was kept minimal; one type of proteoliposome was attached to a nonsticky surface via specific interaction. Comprehensive controls and calibrations demonstrated that *in vitro* fusion activity in bulk solution is preserved in single-liposome fusion on surface. Real-time monitoring of SNARE-mediated, single-liposome fusion has revealed several key features: existence of hemifusion and additional intermediates on the pathway to full fusion and kinetic information on individual intermediate states. Furthermore, our assay might enable the dissection of the different fates of liposomes after fusion, for example, kiss-and-run type detachment. We should, however, emphasize that our work is based on yeast SNAREs and with a

relatively high protein-to-lipid ratio (1:100) and therefore does not yet address the question of whether the SNARE complex is the minimal machinery for fusion (34, 35). We anticipate that our current demonstration will be a starting point for addressing many important issues of SNARE-mediated membrane fusion. One immediate extension would be the adoption of our assay for the neuronal SNARE-complexin-synaptotagmin system (36–39), which may reveal a detailed picture of the  $\text{Ca}^{2+}$ -triggering mechanism in neuronal synapses.

## Materials and Methods

**SNARE Proteins Expression and Purification.** Recombinant SNARE proteins of yeast (26), Sso1pHT, Sec9c, and Snc2pF, were expressed and purified. DNA sequences encoding Sso1pHT (amino acids 185–290) and Snc2pF (amino acids 1–115) were inserted into the pGEX-KG vector between the EcoRI and HindIII sites as N-terminal GST fusion proteins. Sec9c (amino acids 401–651) was inserted into pET-24b(+) between the NdeI and XhoI sites as a C-terminal His<sub>6</sub>-tagged protein. Recombinant GST fusion proteins were expressed in *Escherichia coli* Rosetta (DE3) pLysS (Novagene, San Diego, CA). The cells were grown at 37°C in LB medium with glucose (2 g/liter), ampicillin (100  $\mu\text{g}/\text{ml}$ ), and chloramphenicol (25  $\mu\text{g}/\text{ml}$ ) until the  $A_{600}$  reached 0.6–0.8. Isopropyl- $\beta$ -D-thiogalactopyranoside (IPTG) was added to a final concentration of 0.5 mM. The cells were grown further for 4 h at 18°C. The cell pellets were collected by centrifuge at  $6,000 \times g$  for 10 min then resuspended in resuspension buffer [PBS, pH 7.4, with 0.5% Triton X-100 (vol/vol)] with 2 mM 4-(2-aminoethyl)benzenesulfonyl fluoride (AEBSF). One percent *n*-lauroyl sarcosine was added to the lysate after breaking the cells by sonication on ice bath. The supernatant was mixed with glutathione-agarose beads at 4°C for 2 h after centrifuging the cell lysate at  $15,000 \times g$  for 20 min at 4°C. The protein-bound beads were washed with an excess volume of washing buffer (PBS with 0.2% Triton X-100, pH 7.4), then washed with thrombin cleavage buffer (50 mM Tris-HCl, 150 mM NaCl, 0.8% *n*-octylglucoside, pH 8.0). Finally, the proteins were cleaved from the resin by thrombin (Sigma, St. Louis, MO) at room temperature for 40 min. After elution, AEBSF (2 mM final concentration) was added to stop the cleavage reaction. The His<sub>6</sub>-tagged protein Sec9c was expressed in *E. coli* Rosetta (DE3) pLysS. The cells were grown at 37°C in LB medium with glucose (2 g/liter), kanamycin (30  $\mu\text{g}/\text{ml}$ ), and chloramphenicol (25  $\mu\text{g}/\text{ml}$ ) until the  $A_{600}$  reached 0.6–0.8. After the addition of IPTG (0.5 mM), the cells were grown for 4 h at 30°C. The cell pellets were collected by centrifugation at  $6,000 \times g$  for 10 min and then resuspended in lysis buffer (PBS buffer with 20 mM imidazole, 0.5% Triton X-100, and 2 mM AEBSF, pH 8.0). After sonication on ice, the cell lysate was centrifuged at  $15,000 \times g$  for 20 min at 4°C. The supernatant was mixed with nickel-nitrilotriacetic acid-agarose beads (Qiagen, Valencia, CA) in lysis buffer. The mixture was nutated for binding at 4°C for 1.5 h. After binding, the beads were washed with washing buffer (PBS buffer with 50 mM imidazole, pH 8.0). Then the protein was eluted by elution buffer (PBS buffer with 250 mM imidazole, pH 8.0). All purified proteins were examined with 15% SDS/PAGE.

**Reconstitution of SNARE Proteins in Liposomes.** Unilamellar liposomes containing 65:35 (mol/mol) 1-palmitoyl-2-oleoyl-*sn*-glycero-3-phosphocholine (POPC)/1,2-dioleoyl-*sn*-glycero-3-[phospho-L-serine] (DOPS) (all purchased from Avanti Polar Lipids, Birmingham, AL) labeled with 2 mol% DiI (Molecular Probes/Invitrogen, Carlsbad, CA) were formed by using the extrusion method (MiniExtruder, Avanti Polar Lipids). Sso1pHT was then reconstituted in the liposomes through dialysis. Snc2pF was reconstituted in the same way except that unilamellar liposomes were doped with 2 mol% DiD (Molecular Probes) and 0.1 mol% biotinylated lipids, 1,2-dipalmitoyl-*sn*-glycero-3-phosphoethanolamine-*N*-(biotinyl) (Avanti Polar Lipids). The fluorescence spectra

of DiI and DiD show high similarity to those of Cy3 and Cy5 that are widely used for single-molecule FRET studies (23–25). For membrane reconstitution, proteins were mixed with liposomes at 1:100 protein-to-lipid molar ratio with  $\approx 0.8\%$  *n*-octylglucoside in buffer at room temperature for 20 min. Then the mixture was diluted two times with dialysis buffer [25 mM Hepes/100 mM KCl/3% (wt/vol) glycerol, pH 7.4], after dialysis against 2 liters of dialysis buffer at 4°C overnight. After dialysis, the liposome was treated with SM-2 beads and centrifuged at  $10,000 \times g$  for 5 min to remove protein and lipid aggregates.

**Single-Liposome Fusion Fluorescence Spectroscopy.** A quartz slide was coated with 99:1 (mol/mol) PEG/biotin-PEG (Nektar, Huntsville, AL) to eliminate nonspecific binding of liposomes. The quartz slide was then placed at the bottom of a flow chamber and coated with neutravidin. The Snc2pF-reconstituted liposomes were immobilized on the slide through incubation at 160 pM [liposome] for 15 min via specific biotin–neutravidin binding. The Sso1pHT proteoliposomes were mixed with preset amounts of Sec9c that gives Sec9c/Sso1pHT (mol/mol) = 1:1 or 2:1, diluted to a final liposome concentration of 100 pM (corresponding to one proteoliposome in  $10 \mu\text{m}^3$  volume), and injected into the flow chamber to induce fusion on the surface. In the case of fusion in bulk solution, we mixed the Snc2pF- and the Sso1pHT-reconstituted liposomes; 1:1 (mol/mol) and both at 100 pM, with the required amount of Sec9c. The low concentration of the v- and the t-SNARE liposomes minimized multiple rounds of fusion within the reaction time of 30 min. All measurements were made at  $37 (\pm 2)^\circ\text{C}$  in a buffer (25 mM Hepes, pH 7.4/100 mM KCl).

Single fusion events were monitored in a wide-field total-internal-reflection fluorescence microscope by using an electron multiplying charge-coupled device camera. Details of the wide-field total-internal-reflection fluorescence microscope have been reported (23). Briefly, an area of  $\approx 50 \times 100 \mu\text{m}^2$  was imaged by using an inverted microscope (IX70, Olympus, Melville, NY) that was excited by a frequency-doubled Nd:YAG laser (532 nm; Crystalaser, Reno, NV). The excitation beam was focused into a small pellin broca prism (CVI Laser, Albuquerque, NM), which was placed on top of a quartz slide with a thin layer of immersion oil in between

to match the index of refraction. By changing the incident angle of the excitation beam, the total internal reflection at the interface between the quartz slide and aqueous imaging buffer was achieved. Fluorescence signal was collected with a high NA water immersion objective (UPLAPO60XW; Olympus), and the scattered laser light was rejected by a 550-nm long-pass interference filter (E550LP; Chroma Technology, Rockingham, VT). A dichroic mirror with a reflection range of 550- to 630-nm (645DCXR; Chroma Technology) separated the collected fluorescence signal into two beams having different wavelengths, that is, the donor (550–630 nm) and the acceptor (645 nm and above) channels. These two beams were focused on the electron-multiplying charge-coupled device camera (iXon DV 887-BI; Andor Technology, South Windsor, CT). Fluorescence signal was recorded in real time by using Visual C++ software (Microsoft, Redmond, WA) (the program written by Sean A. McKinney) with time resolution of 100 or 900 ms. Each single fusion event was visually identified and analyzed by using programs written in IDL (Research Systems, Boulder, CO).

One example of such identified single fusion events is shown in SI Movie 1. A program written in MATLAB (Mathworks, Natick, MA) generated the time trajectories of the donor and the acceptor fluorescence intensities and calculated the corresponding FRET efficiency (see the lower panels in SI Movie 1) by using the equation,  $I_A/(I_D + I_A)$ , where  $I_D$  and  $I_A$  are the donor and the acceptor fluorescence intensities, respectively. The average donor and acceptor fluorescence intensities measured before docking were considered as the background fluorescence for each fusion event and subtracted uniformly from the fluorescence signals. The leakage of donor fluorescence into the acceptor channel ( $\approx 17.5\%$  of the total intensity) was then taken into account. Intermediate states of the fusion event, appearing as plateaus in FRET efficiency changes, were visually identified, and the corresponding FRET efficiencies and the dwell times were calculated by using the program written in MATLAB.

This work was supported by National Institutes of Health Grants GM074526 (to T.H.) and GM067629 (to Y.-K.S.) T.-Y.Y. was partially supported by Korea Research Foundation Fellowship M01-2005-000-10293-0. T.H. is an Investigator with the Howard Hughes Medical Institute.

1. Chanturiya A, Chernomordik LV, Zimmerberg J (1997) *Proc Natl Acad Sci USA* 94:14423–14428.
2. Fix M, Melia TJ, Jaiswal JK, Rappoport JZ, You D, Söllner TH, Rothman JE, Simon SM (2004) *Proc Natl Acad Sci USA* 101:7311–7316.
3. Bowen ME, Weninger K, Brunger AT, Chu S (2004) *Biophys J* 87:3569–3584.
4. Liu T, Tucker WC, Bhalla A, Chapman ER, Weisshaar JC (2005) *Biophys J* 89:2458–2472.
5. Melikyan GB, Bamad RJO, Abrahamyan LG, Mothes W, Young JAT (2005) *Proc Natl Acad Sci USA* 102:8728–8733.
6. Rothman JE (1994) *Nature* 372:55–63.
7. Lin RC, Scheller RH (2000) *Annu Rev Cell Dev Biol* 16:19–49.
8. Jahn R, Lang T, Südhof TC (2003) *Cell* 112:519–533.
9. Weber T, Zemelman BV, McNew JA, Westermann B, Gmachl M, Parlati F, Söllner TH, Rothman JE (1998) *Cell* 92:759–772.
10. Poirier MA, Xiao W, Macosko JC, Chan C, Shin Y-K, Bennett MK (1998) *Nat Struct Biol* 5:765–769.
11. Bryan Sutton R, Fasshauer D, Jahn R, Brunger AT (1998) *Nature* 395:347–353.
12. Xu Y, Zhang F, Su Z, McNew JA, Shin Y-K (2005) *Nat Struct Mol Biol* 12:417–422.
13. Giraudo CG, Hu C, You D, Slovic AM, Mosharov EV, Sulzer D, Melia TJ, Rothman JE (2005) *J Cell Biol* 170:249–260.
14. Reese C, Heise F, Mayer A (2005) *Nature* 436:410–414.
15. Lu X, Zhang F, McNew JA, Shin Y-K (2005) *J Biol Chem* 280:30538–30541.
16. Bhalla A, Chicka MC, Tucker WC, Chapman ER (2006) *Nat Struct Mol Biol* 13:323–330.
17. Kemble GW, Danielli T, White JM (1994) *Cell* 76:383–391.
18. Chernomordik LV, Frolov VA, Leikina E, Bronk P, Zimmerberg J (1998) *J Cell Biol* 140:1369–1382.
19. Zaitseva E, Mittal A, Griffin DE, Chernomordik LV (2005) *J Cell Biol* 169:167–177.
20. Earp LJ, Delos SE, Park HE, White JM (2005) *Curr Top Microbiol Immunol* 285:25–66.
21. Lee J, Lentz BR (1997) *Biochemistry* 36:6251–6259.
22. Chernomordik LV, Kozlov MM (2005) *Cell* 123:375–382.
23. Joo C, McKinney SA, Nankura M, Rasnik I, Myong S, Ha T (2006) *Cell* 126:515–527.
24. Myong S, Rasnik I, Joo C, Lohman TM, Ha T (2005) *Nature* 437:1321–1325.
25. Zhuang X, Bartley LE, Babcock HP, Russell R, Ha T, Herschlag D, Chu S (2000) *Science* 288:2048–2051.
26. Rossi G, Salminen A, Rice LM, Brunger AT, Brennwald P (1997) *J Biol Chem* 272:16610–16617.
27. Nakada C, Ritchie K, Oba Y, Nakamura M, Hotta Y, Iino R, Kasai RS, Yamaguchi K, Fujiwara T, Kusumi A (2003) *Nat Cell Biol* 5:626–632.
28. Chernomordik LV, Kozlov MM (2003) *Annu Rev Biochem* 72:175–207.
29. Blanchard SC, Kim HD, Gonzalez RL, Jr, Puglisi JD, Chu S (2004) *Proc Natl Acad Sci USA* 101:12893–12898.
30. Aravanis AM, Pyle JL, Tsien RW (2003) *Nature* 423:643–647.
31. Jackson MB, Chapman ER (2006) *Annu Rev Biophys Biomol Struct* 35:135–160.
32. Cohen FS, Melikyan GB (2004) *J Membr Biol* 199:1–14.
33. Reese C, Mayer A (2005) *J Cell Biol* 171:981–990.
34. Chen X, Araç D, Wang T-M, Gilpin CJ, Zimmerberg J, Rizo J (2006) *Biophys J* 90:2062–2074.
35. Dennison SM, Bowen ME, Brunger AT, Lentz BR (2005) *Biophys J* 90:1661–1675.
36. Schaub JR, Lu X, Doneske B, Shin Y-K, McNew JA (2006) *Nat Struct Mol Biol* 13:748–750.
37. Südhof TC (2004) *Annu Rev Neurosci* 27:509–547.
38. Giraudo CG, Eng WS, Melia TJ, Rothman JE (2006) *Science* 313:676–680.
39. Tang J, Maximov A, Shin O-H, Dai H, Rizo J, Südhof TC (2006) *Cell* 126:1175–1187.